Sampling Bottleneck in Validating Membrane Dynamics

Milka Doktorova[1]*, George Khelashvili[2,3], Michael F. Brown[4-6]*

[1] *Department of Molecular Physiology & Biological Physics, University of Virginia School of Medicine, Charlottesville, VA, USA*
[2] *Department of Physiology and Biophysics, Weill Cornell Medical College of Cornell University, New York, NY, USA*
[3] *Institute of Computational Biomedicine, Weill Cornell Medical College of Cornell University, New York, NY, USA*
[4] *Department of Chemistry and Biochemistry, University of Arizona, Tucson, AZ, USA*
[5] *Department of Physics, University of Arizona, Tucson, AZ, USA*
[6] *Program in Applied Mathematics, University of Arizona, Tucson, AZ, USA*
* *Corresponding authors*
md4xm@virginia.edu, *mfbrown@u.arizona.edu*

ABSTRACT

Molecular dynamics (MD) simulations have become increasingly impactful in membrane biophysics because they offer atomistic resolution into the atomistic fluctuations of lipid assemblies. Validation of the simulation trajectories with experimental data is crucial for interpretation and application of MD results. As an ideal benchmarking technique, NMR spectroscopy delivers order parameters of the carbon–deuterium bond fluctuations along the lipid chains. Additionally, NMR relaxation can access lipid dynamics providing yet another point for validation of simulation force fields. Here we performed short resampling simulations of membrane trajectories to investigate the lipid CH bond fluctuations on sub-40-ps timescales to explore the local fast dynamics. We recently established a robust framework for analysis of NMR relaxation rates from MD simulations, which improves upon current approaches and shows excellent agreement of experimental and theoretical results. The calculation of relaxation rates from simulations presents a universal challenge that we addressed by hypothesizing the existence of fast CH bond dynamics that evade the analysis of simulation data with temporal resolution of 40 ps (or lower). Indeed, our results support this hypothesis confirming the validity of our solution to the sampling problem. Furthermore, we show that the fast CH bond dynamics occur on timescales at which carbon–carbon bond conformations appear nearly stationary and unaffected by cholesterol. Lastly, we discuss the correspondence to the CH bond dynamics of liquid hydrocarbons and relate their existence to the apparent microviscosity of the bilayer hydrocarbon core.

STATEMENT OF SIGNIFICANCE

Nuclear magnetic resonance data have been historically used to validate membrane simulations through the average order parameters of the lipid chains. However, the bond dynamics that give rise to this equilibrium bilayer structure have rarely been compared between in vitro and in silico systems despite the availability of substantial experimental data. Here we investigate the logarithmic timescales sampled by the lipid chain motions and confirm a recently developed computational protocol that creates a dynamics-based bridge between simulations and NMR spectroscopy. Our results establish the foundations for validating a relatively unexplored dimension of bilayer behavior and thus have far-reaching applications in membrane biophysics.

INTRODUCTION

The function of membrane-associated macromolecules is inextricably coupled to the structural and dynamical properties of the lipid bilayer matrix. Various experimental techniques have been developed to probe the relevant conformational and energetic landscapes of lamellar lipid assemblies, and their dependence on both internal (e.g., lipid composition) and external (e.g., temperature, pressure) factors (1-4). For instance, small-angle scattering (SAXS and SANS) data have characterized parameters such as bilayer thickness and area per lipid (5); fluorescence microscopy (6), fluorescence resonance energy transfer (FRET) (7), and cryogenic electron microscopy (cryo-EM) (8,9) have revealed lateral inhomogeneities and phase coexistence in lipid mixtures; flicker spectroscopy (10,11) and neutron spin-echo measurements (12-14) have reported on bilayer elasticity; and fluorescence correlation spectroscopy has quantified lipid diffusion in various contexts (15,16).

While such results have shaped our understanding of the thermodynamic properties of lipid mixtures over a wide range of length- and timescales, the inability of experimental approaches to unambiguously access the conformational dynamics of individual lipid molecules has created room for computational and theoretical investigations (17-19). In particular, molecular dynamics (MD) simulations have been instrumental in uncovering otherwise inaccessible molecular mechanisms of experimental observations occurring at the nanoscale (17-21). Some examples include the role of membrane deformation in the ability of gramicidin to accelerate lipid flip-flop between leaflets (22), the indirect effect of cholesterol on the electrostatics-driven binding of proteins to the membrane (23), the contributions of interleaflet coupling to phase separation (24), and the path taken by a lipid spontaneously flipping to the opposite leaflet (25). Often perceived as a computational microscope, MD simulations have also enabled the unifying comparison of different experimental techniques, as well as guided the refinement of models often critical for the analysis of experimental data in terms of physics-based forces and potentials (5,26).

The versatility of MD simulations in addressing biophysical questions hinges upon the robust validation of the simulation trajectories against increasingly stringent experimental data (2,12,27). In particular, studies related to membrane structure and dynamics rely heavily on the accurate parameterization of the physics-based interatomic interactions (20,28-30). Such sets of parameters, or lipid force fields that govern the bilayer equilibrium and dynamical properties, have been developed for both atomic and coarse-grained molecular models, and optimized against bilayer structural parameters obtained mostly from scattering (SAXS and SANS) and solid-state NMR measurements. Ongoing refinements of the force field parameters have proven successful in reproducing certain aspects of the experimental data, while missing others thus illustrating the inherent need for more points of comparison with experiments (26). In that respect, membrane dynamics present a promising yet relatively less understood fourth dimension of bilayer biophysics – one that can link in vitro measurements of model membranes to the actual lipid motions in simulated systems.

We recently showed that relaxation rates of carbon–deuterium bonds of the lipid acyl chains obtained from NMR spectroscopy can be directly compared to the analogous carbon–hydrogen bond motions in simulated bilayers by means of the spectral densities of the fluctuations (19). While quantifying the CH bond reorientations in the trajectories requires only knowledge of the changes in atomic positions over time, calculating the respective spectral densities necessitates a

Fourier transform of the autocorrelation function of the fluctuations. This calculation turns out to be particularly challenging due to the discrete nature of the simulation data, calling into question the general applicability of this validation approach. Here we describe the problem and its origins (31-34), and demonstrate the validity of a workaround approach that circumvents the sampling issues (19) without the need for additional data.

METHODS

Simulation protocol. We investigated the properties of two fully atomistic lipid bilayers: 1,2-dimyristoyl-*sn*-glycero-3-phosphocholine (DMPC) and DMPC/cholesterol 70/30 mol%. Each bilayer contained 100 lipids per leaflet (200 lipids total) and 45 water molecules per lipid with no added salt ions. The bilayers were simulated in the NPT ensemble at a constant temperature of 317 K (44°C). The original 2 μs-long trajectories, performed with OpenMM (35) and the CHARMM36 force field for lipids (20), were taken from (19). These simulations employed a timestep of 2 fs and atomic coordinates were saved every 40 ps. To analyze the dynamics at shorter length scales, here we resampled these trajectories by restarting the simulation at different time points and running short simulations with more frequent data output. In particular, starting at 0.8, 1.0, 1.2, 1.4, 1.6, 1.8, and 2.0 μs of the original trajectories we ran 400-ps-long simulations by storing atomic coordinates every 10 fs. These resampling simulations were performed with the same simulation parameters as the original long trajectories as described in detail in (19), with the only difference being the 10 fs (instead of 40 ps) data output.

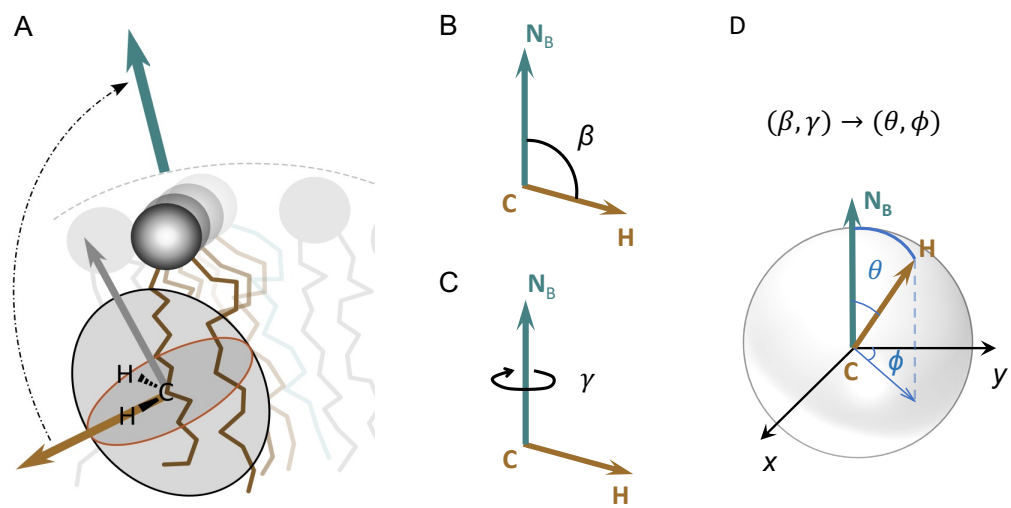

Figure 1. Schematic illustration of the angles used to analyze the bilayer dynamics. (A) Representation of a carbon–hydrogen bond on a lipid chain. (B) The Euler angle β is the angle that the CH bond makes with the bilayer normal, or director axis, $\mathbf{N}_B$. (C) The Euler angle γ defines the rotation of the CH bond around N_B and is calculated as described in (19). (D) The CH bond orientation with respect to the director axis $\mathbf{N}_B$ can be defined in an analogous way in spherical polar coordinates with the angles θ and ϕ.

Analysis of CH bond fluctuations. The fluctuations of the lipid acyl chain carbon-hydrogen (CH) bonds were analyzed following the protocol in (19). Briefly, the instantaneous orientation of a CH bond was described by the two Euler angles β and γ where β defines the angle that the CH bond makes with the bilayer normal (director axis) along the z-dimension of the simulation box and γ quantifies the CH bond rotation around the director (Figure 1). The dynamics of the CH bond are then described in the 3D space by three functions of β and γ, the so-called Wigner rotation matrix elements (36), at every time point t, given by:

$$D_{00}^{(2)}(\Omega;\mathrm{t}) = \frac{1}{2}(3\cos^2\beta(t) - 1)\,, \tag{1}$$

$$D_{01}^{(2)}(\Omega;\mathrm{t}) = \sqrt{\frac{3}{2}}\sin\beta(t)\cos\beta(t)\,e^{-i\gamma(t)}, \tag{2}$$

$$D_{02}^{(2)}(\Omega;\mathrm{t}) = \sqrt{\frac{3}{8}}\sin^2\beta(t)\,e^{-2i\gamma(t)}\,. \tag{3}$$

The above functions are evaluated for every carbon $\mathrm{C}_{l,s}^{(n)}$ where $1 \le l \le N_\mathrm{L}$ is an individual DMPC lipid (N_L being the total number of DMPC lipids in the bilayer) and $2 \le n \le 14$ is the carbon number on the *sn*-1 ($s = 1$) or *sn*-2 ($s = 2$) chain.

The autocorrelation function of each time series $D_{0\mathrm{p}}^{(2)}(\beta,\gamma;\mathrm{t})$ where $p \in [0,1,2]$ is then given by:

$$G_{p,s}^{(n)}(k) = \frac{1}{2N_\mathrm{L}}\sum_{l}\sum_{i} G_{p,l,s}^{(n,i)}(k) \tag{4}$$

with

$$G_{p,l,s}^{(n,i)}(k) = \frac{1}{N_\mathrm{F}-k}\sum_{t=0}^{N_\mathrm{F}-k-1} D_{0p}^{(2)*}(\beta,\gamma;t)D_{0\mathrm{p}}^{(2)}(\beta,\gamma;t+k) - \left|\langle D_{0p}^{(2)}(\beta,\gamma)\rangle\right|^2. \tag{5}$$

In Eq. 4 the inner summation is over the two hydrogen atoms $i = (1,2)$ at carbon $\mathrm{C}_{l,s}^{(n)}$ and in Eq. 5 the second term is the squared mean of the fluctuations; k is lag time, N_F is total number of trajectory frames (or time points), and $D_{0p}^{(2)*}(\beta,\gamma;t)$ denotes the complex conjugate of $D_{0p}^{(2)}(\beta,\gamma;t)$. At zero lag time, i.e., $k = 0$, the autocorrelation function from Eq. 5 is the variance of $D_{0p}^{(2)}(\beta,\gamma)$, which reads:

$$G_{p,l,s}^{(n,i)}(0) = \langle|D_{0p}^{(2)}(\beta,\gamma)|^2\rangle - |\langle D_{0p}^{(2)}(\beta,\gamma)\rangle|^2 = \mathrm{var}[D_{0p}^{(2)}(\beta,\gamma)]. \tag{6}$$

The spectral density function of the fluctuations is the Fourier transform of the autocorrelation function from Eq. 4 and can be calculated as follows:

$$J_{p,s}^{(n)}(\omega) = \sum_{k=0}^{N_F/2-1} G_{p,s}^{(n)}(k) \cos \omega t_k \, \Delta t. \tag{7}$$

In Eq. 7 ω is related to the Larmor frequency ν of the NMR instrument via $\omega = 2\pi\nu$, Δt is the sampling time interval, and $t_k = k\Delta t$ is the time at lag k. The relaxation rate of the fluctuations is a linear combination of $J_{p,s}^{(n)}(\omega)$ evaluated at two specific frequencies, ν and 2ν (19).

Calculation of effective correlation time of the fluctuations. The correlation times of the CH bond fluctuations are described by the functions in Eqs. 1–3 and can be obtained from the corresponding autocorrelation functions $G_{p,s}^{(n)}(k)$ from Eq. 4. However, in general a broad distribution of correlation times is to be expected for either collective or noncollective lipid bilayer motions (31). For a more recent discussion please see Refs. (34,37). In the case of lipid motions, we follow the approach of Giovanni Lipari and Attila Szabo (38) where the effective correlation time, τ_{eff}, is related to the integral of $G_{p,s}^{(n)}(k)$ as follows:

$$\tau_{\text{eff}} = \frac{1}{G_{p,s}^{(n)}(0)} \int_0^\infty G_{p,s}^{(n)}(k)\, dk = \frac{1}{\text{var}[D_{0p}^{(2)}(\beta,\gamma)]} \sum_{k=0}^{N_F/2-1} G_{p,s}^{(n)}(k)\, \Delta t. \tag{8}$$

RESULTS

Output frequency of atomic coordinates can introduce an increase in spectral density. To directly compare the CH bond dynamics between simulations and NMR spectroscopy, we calculated NMR relaxation rates from the simulation trajectories. Relaxation rates can be obtained directly from the spectral density of the CH bond fluctuations as described in detail in (19). The spectral density is the Fourier transform of the autocorrelation function of the fluctuations and is given by Eq. 7. In theory, it should be a two-tailed continuous Fourier transform (or CFT) [see Eq. 11 in (19)]. However, simulations are run with a discrete time step Δt_{sim} and atomic coordinates are output at some fixed sampling time interval $\Delta t \geq \Delta t_{\text{sim}}$, making simulation data points spaced Δt time units apart. Consequently, $J_{p,s}^{(n)}(\omega)$ in Eq. 7 is a one-sided and discrete Fourier transform (or DFT).

We can use a one-sided DFT to approximate a two-sided CFT by multiplying the former by a factor of two. Special care must be taken not to overcount the element at lag time 0 which is the largest element of the autocorrelation function. Thus, $J_{p,s}^{(n)}(\omega)$ can be written as follows:

$$J_{p,s}^{(n)}(\omega) = 2\sum_{k=1}^{N_F/2} G_{p,s}^{(n)}(k)\cos\omega t_k\,\Delta t + G_{p,s}^{(n)}(0)\Delta t. \tag{9}$$

The expression in Eq. 9 corresponds to the spectral density evaluated at a single frequency ω. The second term on the right is a product of the initial value ($k = 0$) of the autocorrelation function (also equal to the variance of the CH bond fluctuations, Eq. 6), and the sampling time interval Δt. Because they are both independent of frequency, their product is effectively a constant that is added to the spectral density at every frequency ω. In theory, $\Delta t \to 0$ making this constant infinitesimally small. However, in simulations the choice of Δt is bounded below by the simulation time step Δt_{sim} (usually 2 fs for fully atomistic simulations) but is often orders of magnitude larger, $\Delta t \gg \Delta t_{\text{sim}}$, e.g., pico- or nanoseconds, and is somewhat arbitrary. This can introduce an artificial shift in the spectral density across all frequencies and directly affect the accuracy of the calculated relaxation rates.

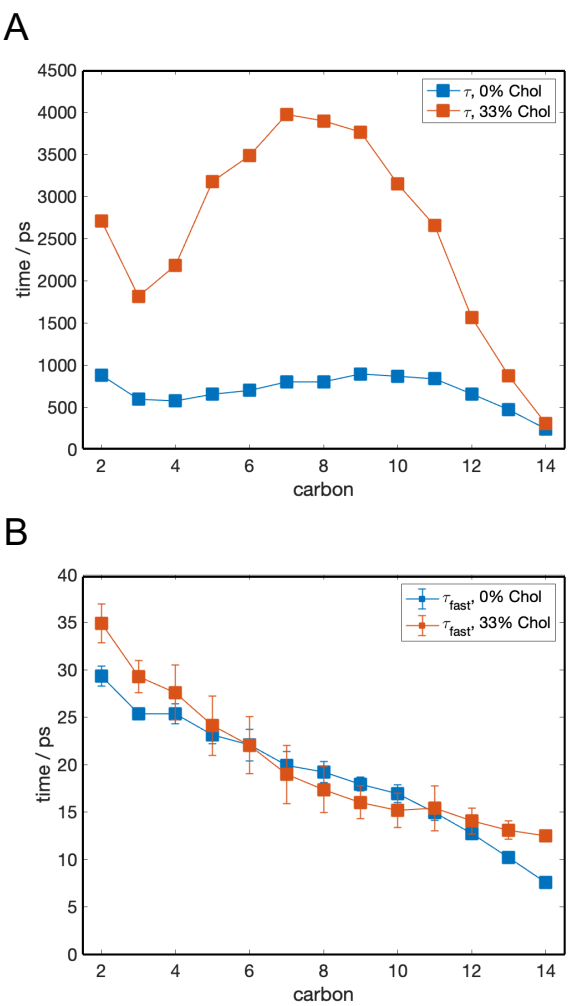

Figure 2. Carbon–hydrogen (CH) bonds exhibit both slow and fast dynamics in fluid DMPC bilayers with 0 and 33 mol% cholesterol. (A) Effective correlation time of CH bond fluctuations calculated from 2-μs-long trajectories with output time interval of 40 ps. (B) Effective correlation time of CH bond fluctuations calculated from short 400-ps-resampling simulations with output time interval of 10 fs. All simulations were performed at 44°C.

Carbon–hydrogen bonds exhibit both slow and fast dynamics in lipid bilayers. According to the Nyquist-Shannon sampling theorem, the discrete Fourier transform in Eq. 9 can accurately represent the underlying continuous Fourier transform if Δt is smaller than half the period of the fastest CH bond motion in the bilayer. To determine the range of CH bond motions in a bilayer, we analyzed the autocorrelation function of their fluctuations in simulation trajectories of DMPC without and with 33 mol% cholesterol from Ref. (19). Following the approach of Lipari and Szabo (38) we calculated the effective correlation time, τ_{eff}, of the CH bond reorientations at all carbons on the *sn*-2 chain of DMPC using Padé approximants (see Methods). Figure 2A shows the results. In the bilayer without cholesterol τ_{eff} was between 0.5 and 1 ns while in the bilayer with cholesterol τ_{eff} reached 4 ns, consistent with the slower dynamics and higher ordering of the CH bonds in the presence of the sterol. In

these simulations, output coordinates were saved every $\Delta t = 40$ ps which according to Figure 2A is smaller than half of τ_{eff}, i.e. $\Delta t < (1/2)\tau_{\text{eff}}$, across all carbons.

To examine the potential contributions of faster dynamics of the CH bonds, e.g., due to bond bending or stretching, we resampled the long simulations by running multiple short simulations with $\Delta t_{\text{rs}} = 10$ fs instead, starting at different time points of the original trajectories as described in Methods. Calculation of τ_{eff} from these resampling simulations showed a much faster reorientation of the CH bonds, $\tau_{\text{eff}}^{\text{fast}}$, occurring on a sub-40-ps timescale (Figure 2B). These fast correlation times ranged between 5 and 35 ps and were independent of cholesterol concentration. Importantly, their existence makes the analysis inconsistent with the Nyquist-Shannon sampling theorem with standard choices of $\Delta t \gg \Delta t_{\text{rs}}$, including the 40-ps output interval employed in the original long trajectories. Instead, using Δt larger than half the period of the fast CH bond dynamics effectively shifts the spectral density to larger values.

Hierarchy of CH bond dynamics can be explained by carbon–carbon bond fluctuations. The CH bond dynamics in NMR and simulations were analyzed with respect to their reorientations relative to the bilayer normal (director axis). To examine the origins of the fast and slow correlation times of their fluctuations, we looked more closely at the dynamics of the carbon–carbon (CC) bonds along the lipid chains. We reasoned that since $\tau_{\text{eff}}^{\text{fast}}$ is not affected by cholesterol it must arise from motions occurring faster than reorientations of whole carbon–carbon segments. To this end, we calculated the dynamics of all covalent CC bonds between carbons C2 and C14 on the *sn*-2 chain of DMPC from the original 2-μs-long trajectories and compared their correlation times to

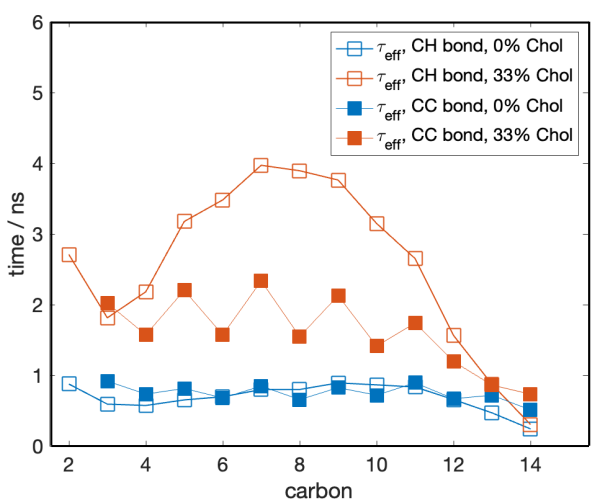

Figure 3. Effective correlation time τ_{CC} of the fluctuations of carbon–carbon (CC) bonds along the *sn*-2 chain of DMPC in the bilayer. Results are shown without (filled blue squares) and with (filled red squared) 33 mol% cholesterol calculated from the original 2-μs-long trajectories with data output every 40 ps. Shown for comparison are the effective (slow) correlation times τ_{CH} of the fluctuations of the CH bonds at the corresponding carbons replotted from Figure 2. All simulations were performed at 44°C.

those of their respective CH bonds. The analysis followed the same protocol described in Methods except that the two Euler angles β and γ defined the orientation of the CC bond, rather than CH bond, with respect to the bilayer normal. Figure 3 shows τ_{eff} for the CC and CH bonds in the bilayers without and with 33 mol% cholesterol. The up-down pattern (even-odd effect) of the CC bond correlation times is expected from the alternating *trans–gauche* isomers of the carbon segments along the lipid chain. Notably, τ_{eff} of the CC bonds is overall very similar to that of the CH bonds. This observation indicates that the slow CH bond dynamics are indeed modulated by the reorientation of their carbon segments (i.e. the two occur on similar timescales) while the fast dynamics happen at time scales relative to which the CC bonds appear stationary.

Sampling problem can be alleviated by resampling the autocorrelation function of the carbon–hydrogen bond fluctuations. The existence of the fast CH bond dynamics presents a challenge for the accurate calculation of a continuous Fourier transform from the discrete simulation data (Eq. 9). This is due to the relatively large time interval employed for outputting atomic coordinates, which prevents adequate sampling of the dynamics of the system according to the Nyquist-Shannon sampling theorem. In other words, the data points of the autocorrelation function of the fluctuations from Eq. 4 are spaced too far apart, making the last constant term on the right in Eq. 9 too large and introducing an artificial increase in the spectral density. One way to alleviate this problem is to reduce Δt as we did in the 400-ps resampling simulations utilizing Δt_{rs} of 10 fs; however the limited sampling in each individual trajectory makes the accurate calculation of relaxation rates challenging.

On the other hand, the autocorrelation function $G_{p,s}^{(n)}(k)$ of the lipid CH bond fluctuations quantified by the Euler angles β and γ and the Wigner rotation matrix elements from Eqs. 1–3, follows a simple mathematical expression (19). In particular, it can be fit to a power-law of the form $ax^b + c$ as shown in Figure 2A in (19). This is important because it allows us to use the best fit $G_{p,s,\mathrm{fit}}^{(n)}$ to resample the correlation function at a much smaller $\Delta t_{\mathrm{fit}} \ll \Delta t$. Since $G_{p,s}^{(n)}(0) = \mathrm{var}[D_{0p}^{(2)}(\beta,\gamma)]$ is the largest element of the autocorrelation function (ACF), we can perform the fit on $G_{p,s}^{(n)}(k)$ for $k \geq 1$ and find the smallest Δt_{fit} that allows the ACF to smoothly approach the variance of the data as $k \to 0$ as shown in Figure 4A. This approach yields Δt_{fit} values between 0 and 30 ps, which are one-half or less than one-half of the corresponding fast correlation times $\tau_{\mathrm{eff}}^{\mathrm{fast}}$ for most carbons (Figure 4B). The recovered spectral density then reads:

$$J_{p,s}^{(n)}(\omega) = 2\sum_{\hat{k}=1}^{N_{F,\mathrm{fit}}} G_{p,s,\mathrm{fit}}^{(n)}(\hat{k}) \cos \omega t_{\hat{k}}\, \Delta t_{\mathrm{fit}} + G_{p,s}^{(n)}(0)\Delta t_{\mathrm{fit}}. \tag{10}$$

According to the Nyquist-Shannon sampling theorem it accurately describes the two-sided continuous Fourier transform/CFT of the correlation function, thus alleviating the sampling problem introduced by the large output interval of atomic coordinates.

DISCUSSION

Both simulations and NMR spectroscopy can detect the motions of the lipid CH bonds in a bilayer. While the actual bond reorientations occur on pico- and nano-second timescales, their relaxation rates at the Larmor frequencies of conventional NMR instruments are in the millisecond regime (31,32,39,40). Simulations give direct access to femto-, pico-, and nanosecond dynamics but can be also used to quantify the millisecond-time relaxation rates of CH bonds from the Fourier transformation of the autocorrelation functions of the bond fluctuation. We recently developed a robust framework that enables this calculation and allows for simulation results to be directly compared to the NMR values. In the process, we discovered a strong dependency of the simulation relaxation rates on the time resolution of the simulation data points, i.e., the output trajectory frames used for the analysis. We hypothesized that the issue was due to the presence of very fast dynamics of the CH bonds, which prevented the accurate calculation of a continuous Fourier

transform with the employed output interval of 40 ps. Here, we directly tested this hypothesis by resampling the simulation trajectories at different time points with short 400-ps-long simulations and an output frequency of 10 fs. The new high-resolution data confirmed the presence of CH bond fluctuations with correlation times between 5 and 35 ps. Further analysis indicated that the hierarchical dynamics are mediated by the fluctuations of the carbon–carbon bonds of the lipid chains. A workaround approach presents a solution to the sampling problem by using a fit to the correlation function to satisfy the conditions of the Nyquist-Shannon sampling theorem (19). Our results thus reveal the presence and source of the very fast CH bond dynamics and establish the validity of resampling their correlation function with the goal of increasing the effective time resolution of the simulation data without any additional simulations.

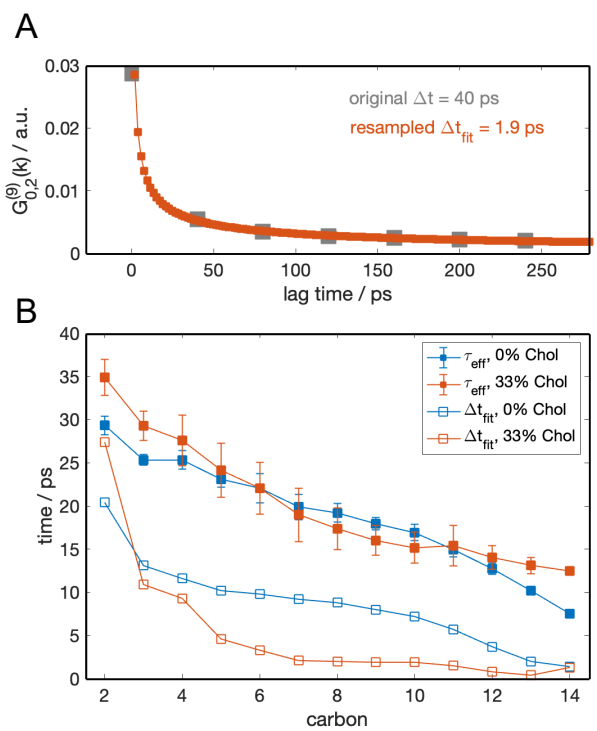

Figure 4. Mathematical resampling of the CH bond autocorrelation function alleviates the sampling problem in the calculation of its Fourier transform. (A) The autocorrelation function of the CH bonds at carbon C9 on the sn-2 chain of DMPC in the bilayer with 33 mol% cholesterol, $G_{0,2}^{(9)}(k)$, calculated every 40 ps from the original long trajectories (gray) and resampled every 1.9 ps from the best power-law fit to $G_{0,2}^{(9)}(k)$ (red). (B) The smallest resampling time interval Δt_{fit} obtained from the best fits to the autocorrelation functions $G_{0,2}^{(i)}(k)$ for carbons $2 \leq i \leq 14$ in the two simulations (open symbols). Shown for comparison are the fast correlation times τ_{fast} for the corresponding CH bonds calculated from short resampling simulations with output time interval of 10 fs and replotted from Figure 2B. All simulations were performed at 44°C.

Output frequency of atomic coordinates. In recent years computational resources have become more easily accessible by researchers and educators, as in the case of graphics processing units (GPUs) used in gaming applications. This has been facilitated by the establishment of large supercomputing infrastructures made available to the public via open proposal calls and freely available training programs on their use. As a result, microsecond-long simulations have become standard even for relatively large fully atomistic systems (41). The decision of how often to output atomic coordinates during a simulation determines both the amount of space needed to store the trajectory files and the maximum time resolution of any subsequent analyses. For instance, an all-atom bilayer with 200 lipids and 45 water molecules per lipid amounts to about 50,000 atoms. Simulating this system for 10 μs would require roughly 200 GB of storage if coordinates are output every 40 ps and 200 TB of disk space if the data output Δt is 40 fs. Therefore, the time resolution needs to be balanced with practical considerations and simultaneous access to sub-picosecond and microsecond dynamics is often challenging.

On the other hand, small windows at faster dynamics can be created by resampling long trajectories via short simulations with smaller $\Delta t_{\mathrm{rs}} < \Delta t$ (42). While this approach provides access to faster

molecular motions, the statistics are limited, and the results are strongly dependent on the state of the bilayer at the chosen starting points for resampling. Lipids can take ~100 ns to exchange places with their nearest neighbor and tens of hundreds of nanoseconds to equilibrate their lateral distribution, even in a simple binary mixture (43). Thus, on the timescale of 400 ps for example, corresponding to the short resampling simulations we performed here, the overall lipid organization in the bilayer remains the same. Therefore, reducing Δt as a way to increase the resolution of the CH bond autocorrelation function and facilitate the accurate calculation of its Fourier transform is often not feasible. Whenever possible, a better approach is to achieve this via mathematical manipulations instead.

Proposed solution and its applicability. To increase the effective sampling of the simulation data, we take advantage of the shape of the CH bond autocorrelation function. When the orientation of the CH bonds is defined with the Wigner rotation matrix elements from Eqs. 1–3, the autocorrelation function (ACF) of their fluctuations (Eq. 4) follows a power-law function (19). Fitting data to the ACF then allows us to sample it at a much smaller $\Delta t_{\mathrm{fit}} \ll \Delta t$, alleviating the dependence of its Fourier transform on the arbitrary choice of Δt. While Δt_{fit} is bounded below by the smooth transition of the ACF fit to the element at lag time $t = 0$, i.e., the variance of the fluctuations (Eq. 6), it is still small enough to satisfy the Nyquist-Shannon sampling theorem, as it is less than half of the fast correlation times we calculated for the CH bonds at most carbons (Figure 4B). This reduces the artificial Δt-dependent shift in the spectral density (Eq. 10), producing relaxation rates in very good agreement with NMR results (Figure 6 in (19)).

Here we quantified the CH bond orientation with respect to the bilayer normal (director axis) with the Euler angles β and γ in Cartesian space, but this can also be done with the spherical angles θ and ϕ in a similar way (Figure 1C). However, it is important to note that this representation and the corresponding correlation function are different from the ones commonly used in the analysis of CH bond relaxation rates from simulations (see Figure 8A and Eqs. 22–24 in (19)). There, the only relevant angle defines the change in the relative direction of the CH bond over time, thus obviating the dependence on the bilayer director axis and the order parameters (19,31). The resulting correlation function obtained from the spherical harmonics addition theorem is equal to 1 at lag time 0 and does not follow a simple functional form. Notably, this prevents the application of the workaround approach we used here, which relies on a fit to the correlation function. As previously discussed (19), the relaxation rates calculated with this approach not only suffer from the same sampling problem, but are also inapplicable to the dynamics of CH bonds of lipids in a bilayer, as they are based on theory coming from solution NMR spectroscopy, which assumes fully isotropic motion.

Fast carbon–hydrogen bond dynamics are universal descriptors of bilayer microviscosity. To continue further, the source of the sampling problem in the Fourier transformation of the CH bond correlation function is the presence of very fast reorientations of the bonds relative to the time resolution of the simulation data points. We see that they have correlation times of less than 40 ps (Figure 2B) and become faster towards the ends of the chains at the bilayer midplane, in agreement with observations made thirty years ago by Richard Pastor et al. from simulations shorter than our resampling trajectories (44) consistent with NMR findings (45). In addition, we also find that these fast motions are independent of cholesterol concentration in the membrane implying that they are not influenced by bulk bilayer properties. In contrast, the

CH bonds also exhibit slower dynamics with correlation times that are orders of magnitude larger than $\tau_{\text{eff}}^{\text{fast}}$ and are thus more easily discoverable with current standard choices for the time step of outputting atomic coordinates. These slower dynamics have a more complicated dependence on chain carbon depth within the bilayer and are strongly influenced by the ordering effects of cholesterol (12).

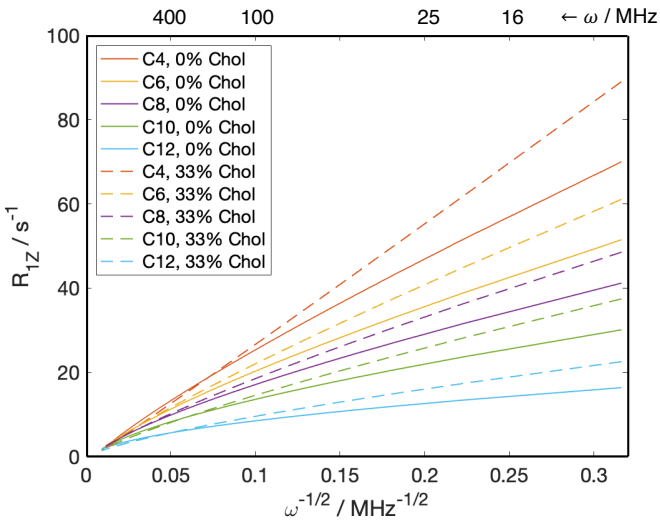

Figure 5. Fast carbon–hydrogen fluctuations are universal descriptors of the bilayer microviscosity. Relaxation rates of CH bonds at carbons 4, 6, 8, 10, and 12 on the *sn*-2 chain of DMPC in the bilayers with 0 and 33 mo% cholesterol as a function of the inverse square root of the Larmor frequency ω. Irrespective of lipid composition, the relaxation rates at all carbons converge at infinite frequency (or infinitesimally small lag time) indicating that the fast correlation times of the CH bonds are universal descriptors of the inherent properties of the bilayer hydrocarbon environment corresponding to the local hydrocarbon microviscosity.

The ability to access logarithmic time-scales in our simulations via the resampling approach allows us to analyze the origins of the fast CH bond dynamics. Our analysis indicates that these fast dynamics occur on timescales at which the carbon–carbon bonds along the acyl chains appear stationary (Figure 3). That can explain why the resulting correlation times are the same within error for bilayers with and without cholesterol, i.e., they are not affected by the structural and dynamical effects induced on the lipids by the sterol. However, as discussed above, the resampling simulations provide only limited statistics due to their short length scales. To further confirm the universality of the fast CH bond dynamics, we can analyze the respective changes in relaxation rates as a function of inverse frequency (Figure 5). Being a signature of the spectral density, the relaxation rate at a given frequency (ω) describes the extent of correlation of the bond fluctuations on that timescale ($t \approx 1/\omega$). At all carbons on the lipid chains, both in the presence and absence of cholesterol, the CH bond relaxation rates differ at relatively small frequencies (or larger $\omega^{-1/2}$ as $t \to \infty$) and converge at infinite frequency as $t \to 0$ indicating that the underlying fast motions of the bonds are similarly correlated across all datasets at very short timescales (Figure 5). In fact, NMR analysis (31,45,46) shows that this common relaxation rate at infinite frequency is the same as that of simple liquid hydrocarbons in solution (not in a bilayer), suggesting that the fast dynamics are a signature of the local bilayer viscosity, or microviscosity, coming from the hydrocarbon environment (44). The same conclusion was made from direct comparison of the fast CH bond dynamics in a 1,2,-dipalmitoyl-*sn*-glycero3-phosphocholine (DPPC) bilayer to those of neat hexadecanes, i.e., hydrocarbons of the same length as the lipid chains but in solution instead of a bilayer. Towards the ends of the lipid chains the CH bonds in the DPPC bilayer have the same correlation times as those of the equivalent carbon positions in hexadecane. However, the CH bonds at the top of the DPPC chains move much slower than those of hexadecane suggesting that the dynamics in that region are strongly influenced by the interfacial tension at the bilayer surface. These observations indicate that the CH bonds of lipids in a bilayer do indeed experience the same

microviscosity as liquid hydrocarbons but only when sufficiently far from the bilayer/water interface.

Validation of membrane dynamics with NMR spectroscopy. As mentioned above, our new and improved framework for the calculation of NMR relaxation rates from simulations addresses not only the sampling bottleneck underlying the discrete Fourier transformation of the correlation function, but also a fundamental problem in the way this calculation has been done in the past. In particular, the theory behind the commonly applied approach for quantifying CH bond relaxation rates from MD trajectories comes from solution NMR which assumes the motion is unrestricted by any ordering potentials (47,48). Contrary to this assumption, both NMR and simulations have clearly demonstrated that the fluctuations of the CH bonds along the lipid chains have distinguishable order parameters, with respect to the bilayer director axis, which directly invalidates the application of the solution NMR result for the case of lipid motions in a bilayer. Stated differently, the presence of the ordering potential introduces a preferred director axis (bilayer normal), relative to which the orientational lipid fluctuations are described by order parameters. The order parameters are the moments of the orientational distribution function (i.e., the partition function) used to calculate bilayer properties using a continuum statistical mechanical approach (49) and are fundamental determinants of the range of CH bond motions. Our new formulation (Eqs. 1–4) thus establishes a direct connection between bilayer lipid dynamics measured in vitro and in silico, providing new avenues for validating the dynamical properties of MD simulations with NMR spectroscopy.

While the absolute relaxation rates at different carbons in the simulations and experiment are directly comparable, additional validation can be carried out against the relationship between CH bond relaxation rates and their respective squared order parameters (31,45,46). We found that the two quantities exhibit a linear dependence, the so-called square-law, which is clearly discernible both in the experimental (50,51) and simulation data (19). The particular dependence of the relaxation rates on the square of the order parameter is related to the $\omega^{-1/2}$ dependence seen in Figure 5 and describes the nature of lipid dynamics (segmental and resembling those of nematic liquid crystals). We also found that this dependence holds specifically for the CH bonds situated far from the lipid/water interface where the two leaflets intercalate [see Figure 5 in (19)]. The unique resemblance of the microviscosity of this bilayer region to that of neat hydrocarbons (whose relaxation rates are independent of frequency), implies that the square-law relationship is an intrinsic property of the bilayer core. Furthermore, the slope of the square-law uniquely corresponds to the local bilayer bending rigidity, thus revealing trends in the elastic behavior of lipid bilayers that are sometimes concealed when measured at long length- and time-scales (12,52). Therefore, validating lipid dynamics with NMR spectroscopy through the square-law dependence provides an unprecedented opportunity to corroborate multiple aspects of membrane biophysical properties captured by the underlying lipid force fields.

CONCLUSION

Molecular dynamics simulations offer a fascinating and detailed first look into the structural and dynamical properties of biological systems. Still, the generality and reliability of the results depends on how well the simulation captures the essential aspects of the processes it models. Being sensitive to the fluctuations of individual carbon–hydrogen bonds in a bilayer, NMR relaxation

provides different points for comparison and validation of the membrane dynamics. Extracting comparable relaxation rates from the simulation trajectories is not trivial, as it relies on complex theoretical concepts and continuous Fourier transformation of discrete simulation data. Notably our new framework successfully tackles these challenges by allowing for replication of experimentally obtained absolute values and trends. It thus helps link the dynamical phenomena observed in vitro to the detailed atomistic motions underlying it, thereby assisting the interpretation of NMR results and offering a deeper appreciation of the biophysics of lipid membranes.

ACKNOWLEDGMENTS

M.D. is supported by NIH postdoctoral fellowship F32GM134704. G.K. is supported by the HRH Prince Alwaleed Bin Talal Bin Abdulaziz Alsaud Institute of Computational Biomedicine at Weill Cornell Medical College through the 1923 Fund. M.F.B. acknowledges NIH support through grant R01EY026041 and NSF through grants MCB 1817862 and CHE 1904125. Molecular dynamics simulations were performed using the Oak Ridge Leadership Computing Facility (Summit allocation BIP109) at the Oak Ridge National Laboratory (supported by the Office of Science of the U.S. Department of Energy under Contract No. DE-AC05-00OR22725).

REFERENCES

1. Molugu, T. R., S. Lee, and M. F. Brown. 2017. Concepts and Methods of Solid-State NMR Spectroscopy Applied to Biomembranes. *Chem. Rev.* 117(19):12087-12132, doi: 10.1021/acs.chemrev.6b00619, https://www.ncbi.nlm.nih.gov/pubmed/28906107.
2. Mallikarjunaiah, K. J., J. J. Kinnun, H. I. Petrache, and M. F. Brown. 2019. Flexible lipid nanomaterials studied by NMR spectroscopy. *Phys. Chem. Chem. Phys.* 21(34):18422-18457, doi: 10.1039/c8cp06179c, https://www.ncbi.nlm.nih.gov/pubmed/31410425.
3. Doole, F. T., T. Kumarage, R. Ashkar, and M. F. Brown. 2022. Cholesterol Stiffening of Lipid Membranes. *J Membr Biol*. 255(4-5):385-405, doi: 10.1007/s00232-022-00263-9, https://www.ncbi.nlm.nih.gov/pubmed/36219221.
4. Safinya, C. R., and J. Radler. 2021. Handbook of lipid membranes: molecular, functional, and materials aspects. CRC Press.
5. Heberle, F. A., J. Pan, R. F. Standaert, P. Drazba, N. Kucerka, and J. Katsaras. 2012. Model-based approaches for the determination of lipid bilayer structure from small-angle neutron and X-ray scattering data. *Eur. Biophys. J.* 41(10):875-890, doi: 10.1007/s00249-012-0817-5, http://www.ncbi.nlm.nih.gov/pubmed/22588484
6. Goh, S. L., J. J. Amazon, and G. W. Feigenson. 2013. Toward a better raft model: modulated phases in the four-component bilayer, DSPC/DOPC/POPC/CHOL. *Biophys. J.* 104(4):853-862, doi: 10.1016/j.bpj.2013.01.003, http://www.ncbi.nlm.nih.gov/pubmed/23442964
7. Heberle, F. A., J. Wu, S. L. Goh, R. S. Petruzielo, and G. W. Feigenson. 2010. Comparison of three ternary lipid bilayer mixtures: FRET and ESR reveal nanodomains. *Biophys. J.* 99(10):3309-3318, doi: 10.1016/j.bpj.2010.09.064, http://www.ncbi.nlm.nih.gov/pubmed/21081079

8. Heberle, F. A., M. Doktorova, H. L. Scott, A. D. Skinkle, M. N. Waxham, and I. Levental. 2020. Direct label-free imaging of nanodomains in biomimetic and biological membranes by cryogenic electron microscopy. *Proc. Natl. Acad. Sci. U.S.A.* 117(33):19943-19952, doi: 10.1073/pnas.2002200117, https://www.ncbi.nlm.nih.gov/pubmed/32759206.
9. Cornell, C. E., A. Mileant, N. Thakkar, K. K. Lee, and S. L. Keller. 2020. Direct imaging of liquid domains in membranes by cryo-electron tomography. *Proc. Natl. Acad. Sci. U.S.A.* 117(33):19713-19719, doi: 10.1073/pnas.2002245117, https://www.ncbi.nlm.nih.gov/pubmed/32759217.
10. Faizi, H. A., A. Tsui, R. Dimova, and P. M. Vlahovska. 2022. Bending Rigidity, Capacitance, and Shear Viscosity of Giant Vesicle Membranes Prepared by Spontaneous Swelling, Electroformation, Gel-Assisted, and Phase Transfer Methods: A Comparative Study. *Langmuir*. 38(34):10548-10557, doi: 10.1021/acs.langmuir.2c01402, https://www.ncbi.nlm.nih.gov/pubmed/35993569.
11. Usery, R. D., T. A. Enoki, S. P. Wickramasinghe, V. P. Nguyen, D. G. Ackerman, D. V. Greathouse, R. E. Koeppe, F. N. Barrera, and G. W. Feigenson. 2018. Membrane Bending Moduli of Coexisting Liquid Phases Containing Transmembrane Peptide. *Biophys. J.* 114(9):2152-2164, doi: 10.1016/j.bpj.2018.03.026, https://www.ncbi.nlm.nih.gov/pubmed/29742408.
12. Chakraborty, S., M. Doktorova, T. R. Molugu, F. A. Heberle, H. L. Scott, B. Dzikovski, M. Nagao, L. R. Stingaciu, R. F. Standaert, F. N. Barrera, J. Katsaras, G. Khelashvili, M. F. Brown, and R. Ashkar. 2020. How cholesterol stiffens unsaturated lipid membranes. *Proc. Natl. Acad. Sci. U.S.A.* 117(36):21896-21905, doi: 10.1073/pnas.2004807117, https://www.ncbi.nlm.nih.gov/pubmed/32843347.
13. Ashkar, R., M. Doktorova, F. A. Heberle, H. L. Scott, F. N. Barrera, J. Katsaras, G. Khelashvili, and M. F. Brown. 2021. Reply to Nagle et al.: The universal stiffening effects of cholesterol on lipid membranes. *Proc. Natl. Acad. Sci. U.S.A.* 118(20), doi: 10.1073/pnas.2102845118, https://www.ncbi.nlm.nih.gov/pubmed/33952694.
14. Gupta, S., F. T. Doole, T. Kumarage, M. Doktorova, G. Khelashvili, R. Ashkar, and M. F. Brown. 2022. Cholesterol stiffening of lipid membranes and drug interactions: Insights from neutron spin echo and deuterium NMR spectroscopy. In Cholesterol. Elsevier, pp. 771-796.
15. Pinkwart, K., F. Schneider, M. Lukoseviciute, T. Sauka-Spengler, E. Lyman, C. Eggeling, and E. Sezgin. 2019. Nanoscale dynamics of cholesterol in the cell membrane. *The Journal of biological chemistry*. 294(34):12599-12609, doi: 10.1074/jbc.RA119.009683, https://www.ncbi.nlm.nih.gov/pubmed/31270209.
16. Beckers, D., D. Urbancic, and E. Sezgin. 2020. Impact of Nanoscale Hindrances on the Relationship between Lipid Packing and Diffusion in Model Membranes. *J. Phys. Chem. B*. 124(8):1487-1494, doi: 10.1021/acs.jpcb.0c00445, https://www.ncbi.nlm.nih.gov/pubmed/32026676.
17. Pastor, R. W., R. M. Venable, and S. E. Feller. 2002. Lipid bilayers, NMR relaxation, and computer simulations. *Acc. Chem. Res.* 35(6):438-446, doi: 10.1021/ar0100529, https://www.ncbi.nlm.nih.gov/pubmed/12069629.
18. Marrink, S. J., V. Corradi, P. C. T. Souza, H. I. Ingolfsson, D. P. Tieleman, and M. S. P. Sansom. 2019. Computational Modeling of Realistic Cell Membranes. *Chem. Rev.*

119(9):6184-6226, doi: 10.1021/acs.chemrev.8b00460, https://www.ncbi.nlm.nih.gov/pubmed/30623647.

19. Doktorova, M., G. Khelashvili, R. Ashkar, and M. F. Brown. 2023. Molecular simulations and NMR reveal how lipid fluctuations affect membrane mechanics. *Biophys. J.* 122(6):984-1002, doi: 10.1016/j.bpj.2022.12.007, https://www.ncbi.nlm.nih.gov/pubmed/36474442.
20. Klauda, J. B., R. M. Venable, J. A. Freites, J. W. O'Connor, D. J. Tobias, C. Mondragon-Ramirez, I. Vorobyov, A. D. MacKerell, Jr., and R. W. Pastor. 2010. Update of the CHARMM all-atom additive force field for lipids: validation on six lipid types. *J. Phys. Chem. B*. 114(23):7830-7843, doi: 10.1021/jp101759q, https://www.ncbi.nlm.nih.gov/pubmed/20496934.
21. Venable, R. M., F. L. Brown, and R. W. Pastor. 2015. Mechanical properties of lipid bilayers from molecular dynamics simulation. *Chem. Phys. Lipids*. 192:60-74, doi: 10.1016/j.chemphyslip.2015.07.014, https://www.ncbi.nlm.nih.gov/pubmed/26238099.
22. Doktorova, M., F. A. Heberle, D. Marquardt, R. Rusinova, R. L. Sanford, T. A. Peyear, J. Katsaras, G. W. Feigenson, H. Weinstein, and O. S. Andersen. 2019. Gramicidin Increases Lipid Flip-Flop in Symmetric and Asymmetric Lipid Vesicles. *Biophys. J.* 116(5):860-873, doi: 10.1016/j.bpj.2019.01.016, https://www.ncbi.nlm.nih.gov/pubmed/30755300.
23. Doktorova, M., F. A. Heberle, R. L. Kingston, G. Khelashvili, M. A. Cuendet, Y. Wen, J. Katsaras, G. W. Feigenson, V. M. Vogt, and R. A. Dick. 2017. Cholesterol Promotes Protein Binding by Affecting Membrane Electrostatics and Solvation Properties. *Biophys. J.* 113(9):2004-2015, doi: 10.1016/j.bpj.2017.08.055, http://www.ncbi.nlm.nih.gov/pubmed/29117524.
24. Perlmutter, J. D., and J. N. Sachs. 2011. Interleaflet interaction and asymmetry in phase separated lipid bilayers: molecular dynamics simulations. *J. Am. Chem. Soc.* 133(17):6563-6577, doi: 10.1021/ja106626r, https://www.ncbi.nlm.nih.gov/pubmed/21473645.
25. Gurtovenko, A. A., and I. Vattulainen. 2007. Molecular mechanism for lipid flip-flops. *J. Phys. Chem. B*. 111(48):13554-13559, doi: 10.1021/jp077094k, https://www.ncbi.nlm.nih.gov/pubmed/17988118.
26. Doktorova, M., N. Kucerka, J. J. Kinnun, J. Pan, D. Marquardt, H. L. Scott, R. M. Venable, R. W. Pastor, S. R. Wassall, J. Katsaras, and F. A. Heberle. 2020. Molecular Structure of Sphingomyelin in Fluid Phase Bilayers Determined by the Joint Analysis of Small-Angle Neutron and X-ray Scattering Data. *J. Phys. Chem. B*. 124(25):5186-5200, doi: 10.1021/acs.jpcb.0c03389, https://www.ncbi.nlm.nih.gov/pubmed/32468822.
27. Molugu, T. R., R. L. Thurmond, T. M. Alam, T. P. Trouard, and M. F. Brown. 2022. Phospholipid headgroups govern area per lipid and emergent elastic properties of bilayers. *Biophys. J.* 121(21):4205-4220, doi: 10.1016/j.bpj.2022.09.005, https://www.ncbi.nlm.nih.gov/pubmed/36088534.
28. Yu, Y., A. Kramer, R. M. Venable, B. R. Brooks, J. B. Klauda, and R. W. Pastor. 2021. CHARMM36 Lipid Force Field with Explicit Treatment of Long-Range Dispersion: Parametrization and Validation for Phosphatidylethanolamine, Phosphatidylglycerol, and Ether Lipids. *J. Chem. Theory Comput.* 17(3):1581-1595, doi: 10.1021/acs.jctc.0c01327, https://www.ncbi.nlm.nih.gov/pubmed/33620194.

29. Souza, P. C. T., R. Alessandri, J. Barnoud, S. Thallmair, I. Faustino, F. Grunewald, I. Patmanidis, H. Abdizadeh, B. M. H. Bruininks, T. A. Wassenaar, P. C. Kroon, J. Melcr, V. Nieto, V. Corradi, H. M. Khan, J. Domanski, M. Javanainen, H. Martinez-Seara, N. Reuter, R. B. Best, I. Vattulainen, L. Monticelli, X. Periole, D. P. Tieleman, A. H. de Vries, and S. J. Marrink. 2021. Martini 3: a general purpose force field for coarse-grained molecular dynamics. *Nat Methods*. 18(4):382-388, doi: 10.1038/s41592-021-01098-3, https://www.ncbi.nlm.nih.gov/pubmed/33782607.
30. Lee, J., X. Cheng, J. M. Swails, M. S. Yeom, P. K. Eastman, J. A. Lemkul, S. Wei, J. Buckner, J. C. Jeong, Y. Qi, S. Jo, V. S. Pande, D. A. Case, C. L. Brooks, 3rd, A. D. MacKerell, Jr., J. B. Klauda, and W. Im. 2016. CHARMM-GUI Input Generator for NAMD, GROMACS, AMBER, OpenMM, and CHARMM/OpenMM Simulations Using the CHARMM36 Additive Force Field. *J. Chem. Theory Comput.* 12(1):405-413, doi: 10.1021/acs.jctc.5b00935, https://www.ncbi.nlm.nih.gov/pubmed/26631602.
31. Brown, M. F. 1982. Theory of spin-lattice relaxation in lipid bilayers and biological membranes. ^{2}H and ^{14}N quadrupolar relaxation. *Chem. Phys.* 77(3):1576-1599.
32. Nevzorov, A., and M. Brown. 1997. Dynamics of lipid bilayers from comparative analysis of ^{2}H and ^{13}C nuclear magnetic resonance relaxation data as a function of frequency and temperature. *J. Chem. Phys.* 107(23):10288-10310.
33. Leftin, A., and M. F. Brown. 2011. An NMR database for simulations of membrane dynamics. *Biochim. Biophys. Acta*. 1808(3):818-839, doi: 10.1016/j.bbamem.2010.11.027, https://www.ncbi.nlm.nih.gov/pubmed/21134351.
34. Smith, A. A., A. Vogel, O. Engberg, P. W. Hildebrand, and D. Huster. 2022. A method to construct the dynamic landscape of a bio-membrane with experiment and simulation. *Nat. Commun*. 13(1):108, doi: 10.1038/s41467-021-27417-y, https://www.ncbi.nlm.nih.gov/pubmed/35013165.
35. Eastman, P., J. Swails, J. D. Chodera, R. T. McGibbon, Y. Zhao, K. A. Beauchamp, L. P. Wang, A. C. Simmonett, M. P. Harrigan, C. D. Stern, R. P. Wiewiora, B. R. Brooks, and V. S. Pande. 2017. OpenMM 7: Rapid development of high performance algorithms for molecular dynamics. *PLoS Comput Biol*. 13(7):e1005659, doi: 10.1371/journal.pcbi.1005659, https://www.ncbi.nlm.nih.gov/pubmed/28746339.
36. Rose, M. E. 1995. Elementary theory of angular momentum. Courier Corporation.
37. Brown, M. F. 2019. 7 Collective dynamics in lipid membranes. *Characterization of Biological Membranes: Structure and Dynamics*.231-268.
38. Lipari, G., and A. Szabo. 1980. Effect of librational motion on fluorescence depolarization and nuclear magnetic resonance relaxation in macromolecules and membranes. *Biophys. J.* 30(3):489-506, doi: 10.1016/S0006-3495(80)85109-5, https://www.ncbi.nlm.nih.gov/pubmed/7260284.
39. Brown, M. F., and S. I. Chan. 2007. Bilayer Membranes: Deuterium and Carbon-13 NMR. *eMagRes*.
40. Nevzorov, A. A., T. P. Trouard, and M. F. Brown. 1998. Lipid bilayer dynamics from simultaneous analysis of orientation and frequency dependence of deuterium spin-lattice and quadrupolar order relaxation. *Phys. Rev. E*. 58(2):2259.

41. Pezeshkian, W., and S. J. Marrink. 2021. Simulating realistic membrane shapes. *Curr Opin Cell Biol*. 71:103-111, doi: 10.1016/j.ceb.2021.02.009, https://www.ncbi.nlm.nih.gov/pubmed/33721706.
42. Venable, R. M., A. J. Sodt, B. Rogaski, H. Rui, E. Hatcher, A. D. MacKerell, Jr., R. W. Pastor, and J. B. Klauda. 2014. CHARMM all-atom additive force field for sphingomyelin: elucidation of hydrogen bonding and of positive curvature. *Biophys. J.* 107(1):134-145, doi: 10.1016/j.bpj.2014.05.034, https://www.ncbi.nlm.nih.gov/pubmed/24988348.
43. Hong, C., D. P. Tieleman, and Y. Wang. 2014. Microsecond molecular dynamics simulations of lipid mixing. *Langmuir*. 30(40):11993-12001, doi: 10.1021/la502363b, https://www.ncbi.nlm.nih.gov/pubmed/25237736.
44. Venable, R. M., Y. Zhang, B. J. Hardy, and R. W. Pastor. 1993. Molecular dynamics simulations of a lipid bilayer and of hexadecane: an investigation of membrane fluidity. *Science*. 262(5131):223-226, doi: 10.1126/science.8211140, https://www.ncbi.nlm.nih.gov/pubmed/8211140.
45. Brown, M. F., A. A. Ribeiro, and G. D. Williams. 1983. New view of lipid bilayer dynamics from 2H and 13C NMR relaxation time measurements. *Proc. Natl. Acad. Sci. U.S.A.* 80(14):4325-4329, doi: 10.1073/pnas.80.14.4325, https://www.ncbi.nlm.nih.gov/pubmed/6576340.
46. Brown, M. F. 1984. Theory of spin-lattice relaxation in lipid bilayers and biological membranes. Dipolar relaxation. *Chem. Phys.* 80(6):2808-2831.
47. Cavanagh, J., N. J. Skelton, W. J. Fairbrother, M. Rance and A. G. Palmer III. 2006. Protein NMR spectroscopy: principles and practice. 2nd Edition. Academic press.
48. Claridge, T. D. 2016. High-resolution NMR techniques in organic chemistry. Elsevier.
49. Petrache, H. I., S. W. Dodd, and M. F. Brown. 2000. Area per lipid and acyl length distributions in fluid phosphatidylcholines determined by ^{2}H NMR spectroscopy. *Biophys. J.* 79(6):3172-3192, doi: 10.1016/S0006-3495(00)76551-9, https://www.ncbi.nlm.nih.gov/pubmed/11106622.
50. Martinez, G. V., E. M. Dykstra, S. Lope-Piedrafita, C. Job, and M. F. Brown. 2002. NMR elastometry of fluid membranes in the mesoscopic regime. *Phys. Rev. E*. 66(5 Pt 1):050902, doi: 10.1103/PhysRevE.66.050902, https://www.ncbi.nlm.nih.gov/pubmed/12513460.
51. Huber, T., K. Rajamoorthi, V. F. Kurze, K. Beyer, and M. F. Brown. 2002. Structure of docosahexaenoic acid-containing phospholipid bilayers as studied by ^{2}H NMR and molecular dynamics simulations. *J. Am. Chem. Soc.* 124(2):298-309.
52. Lessen, H. J., K. C. Sapp, A. H. Beaven, R. Ashkar, and A. J. Sodt. 2022. Molecular mechanisms of spontaneous curvature and softening in complex lipid bilayer mixtures. *bioRxiv*.2022.2002.2017.480963, doi: 10.1101/2022.02.17.480963, https://www.biorxiv.org/content/biorxiv/early/2022/02/18/2022.02.17.480963.full.pdf.